

Modelling of BST Thin Film Varactors for Wireless Communication Systems

Muhammad Farid Abdul Khalid* and Kay Latham

Abstract— Barium Strontium Titanate (BST) is a versatile material with numerous applications in today's modern technology primarily due to its ferroelectric and dielectric properties. BST thin film varactors are increasingly recognized for their potential in wireless communication applications due to its unique properties, tunability and power handling capability. This paper presents the modelling of a BST thin film varactor on sapphire substrate and, the correlation between its tunability and 1 dB compression point. A parametric analysis was performed to investigate the impact of varying its interdigital capacitor (IDC) geometry on the shape of the nonlinear capacitance-voltage (C-V) curve. Three distinct C-V curves namely narrow, broad and intermediate varactors were determined and their tunabilities and 1 dB compression points were derived. Comparisons were made between the simulated and measured results where the narrow varactor achieved the highest tunability of ~50 % and the broad varactor achieved the highest 1 dB compression point of ~41 dBm. The results demonstrate the potential for these varactors to be incorporated in wireless communication systems.

Index Terms—barium strontium titanate (BST), compression points, interdigital capacitor (IDC), wireless communication systems, tunability

I. INTRODUCTION

Complex-oxide thin films are gaining ground in the development of future wireless communication and information systems. The emergence of ferroelectric materials, in particular barium strontium titanate (BST) which has unique microwave properties of large dielectric tunability and low microwave loss at room temperature, has sparked research interest for the past 30 years [1-3]. One of the major areas where ferroelectric materials can play a significant role is in the RF and microwave systems which are increasingly broadband, leverage digital

solutions, and demand extremely high linearity, seeking also to minimize size, weight, power and cost [4]. The growing demand for higher broadband/bandwidth and multiple channels requires the current and future wireless systems to be more adaptable and reconfigurable.

Ferroelectric materials are attractive to microwave and optical applications due to their physical properties that are sensitive towards external electric, magnetic and mechanical fields as well as to temperature. The physical properties include permittivity, permeability, polarization and refractive index [5]. BST thin film in paraelectric phase exhibits a nonlinear characteristic when an electric field is applied and the physical tuning of its dielectric permittivity is fundamental in realising an electronically tunable microwave component known as a variable capacitor or varactor [6].

The BST thin film varactors have a significant impact on the realisation of many adaptive, flexible and reconfigurable microwave devices such as tunable bandpass filter for single and dual-band SDR front-ends [7], phase shifters for electronically steerable satellite communication and radar systems [8], a switchless quad band filter based on BST FBARs for matching networks [9], a compact wideband antenna utilizing BST nanoparticles as filler [10] and BST for 5G applications [11]. A plethora of research studies have focused on enhancing the tunability and lowering the microwave losses of the varactors to be implemented in these microwave devices. However, only a few research studies have emphasized the large-signal performance of nonlinear BST thin film varactors in which the important device parameters are linearity and power handling capability.

C. Schuster et al. presented a tunable multi-bandstop filter based on commercially available BST thin film varactors which offers higher tunability, higher linearity, good power handling capability and moderate losses compared to conventional tunable bandpass solutions [12]. Other researches from the Institute for Microwave Engineering and Photonics, Technische Universität Darmstadt emphasized mostly on the performance of BST thick films being applied in tunable matching network, high power matching circuits and filters [13-15].

These studies, however, did not emphasize the importance of the 1 dB compression point of BST varactors. More importantly, the relationship between the tunability and the 1 dB compression point of BST thin film varactor has not been studied in detail. The 1 dB compression point is defined as the power level at which the output power of a nonlinear device

This manuscript is submitted on August 27, 2024, revised on September 13, 2024, and accepted on September 18, 2024.

Muhammad Farid Abdul Khalid is with the NANO-ElecTronic Centre (NET), School of Electrical Engineering, College of Engineering, Universiti Teknologi MARA, 40450 Shah Alam, Selangor Malaysia (e-mail: mfarid044@uitm.edu.my).

Kay Latham is with the School of Science, College of Science, Engineering and Health, RMIT University, Melbourne, VIC 3001, Australia (e-mail: kay.latham@rmit.edu.au).

*Corresponding author
Email address: mfarid044@uitm.edu.my

1985-5389/© 2023 The Authors. Published by UiTM Press. This is an open access article under the CC BY-NC-ND license (<http://creativecommons.org/licenses/by-nc-nd/4.0/>).

reduces by 1 dB from its ideal linear response. At this point, the gain response of the device is reduced by 1 dB.

This work aims to develop a correlation between the tunability and 1 dB compression points of BST thin film varactors fabricated on c-plane sapphire substrates. The research objective is to analyse the effect of varying the geometry of the BST interdigital capacitor (IDC) in terms of its finger gap, finger width, finger length and the number of fingers on the shape of the nonlinear C-V curves. The shape of the C-V curves will certainly become narrower or broader, depending on the geometry selections. The relationships between the optimised C-V curves and their 1 dB compression points are subsequently shown by simulations and measurements.

II. MODELLING OF BST INTERDIGITAL CAPACITOR

The BST IDC geometry was initially modelled in Computer Simulation Technology (CST) software with the parameter specifications given in Table I. The same IDC specifications for the 400 nm BST layer was previously fabricated on c-plane sapphire substrates [16]. The measured capacitance values were then used to accurately determine the corresponding dielectric constants from 0 to 40 V for the simulation setup which will be discussed later. In this research, BST thin films were deposited on c-plane sapphire substrates using the Kurt J. Lesker RF magnetron sputterer. A thickness of ~400 nm was consistently achieved in all samples. The samples were then post-annealed in air and IDCs were fabricated on the samples as elaborated in [16], achieving ~50 % tunability and Q_{\max} of ~20 at 10 GHz.

The initial model of the BST varactor on sapphire substrate is shown in Figure 1. The BST interdigital capacitor (IDC) geometry which consisted of finger gap (f_G), finger width (f_W), finger length (f_L) and number of fingers (f_N) was designed on top of a BST layer on sapphire substrate. The values of these parameters are tabulated in Table I. The IDC was designed with perfect electric conductor (PEC) electrodes and pads in an enclosed shielded structure.

Two *full plane* ports were defined and boundary conditions of perfectly electric conducting walls were assigned at each side of the structure as depicted in Figure 2. The size of the waveguide port should be reasonably large enough to incorporate a significant part of the varactor fields. A port size that is too large may cause higher order waveguide modes to propagate in the port which results in very slow energy decays in the transient and sharp spikes in the frequency domain simulations respectively. However, a port size which is too

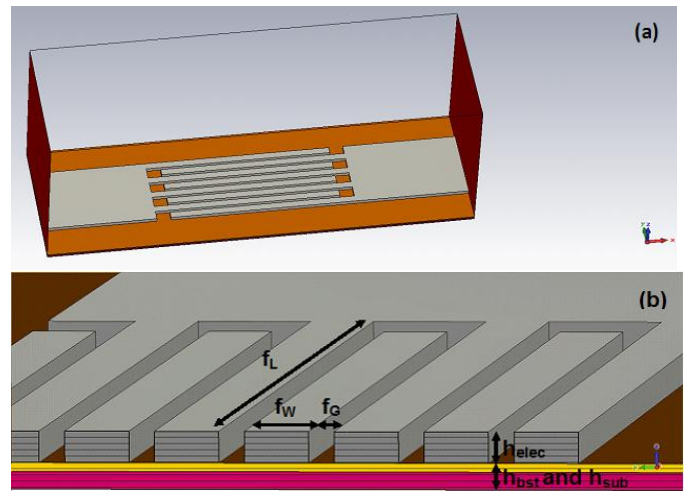


Fig. 1. (a) Side view and (b) cross section of the modelled BST interdigital capacitor geometry.

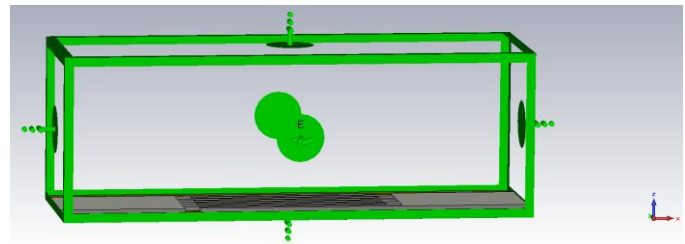


Fig. 2. The boundary conditions with perfect electric conducting walls at each side of the modelled device structure.

small may cause degradation of the S-parameter's accuracy or even instabilities of the transient solver [17]. Therefore, the easiest method of defining the ports which covers the entire boundary face of the device structure is to use the *Full Plane* option.

Depending on the type of structure to be simulated, the *transient (time domain) solver* and *frequency domain solver* are typically chosen to calculate the S-parameters. A *transient solver* is more suitable to simulate any kind of S-parameter or antenna problem and with the broadband simulation, the S-parameters for the entire desired frequency range could be achieved. The *frequency domain solver* is the fastest tool when it comes to calculating a small number of frequency samples and, to reduce simulation time, a broadband S-parameter simulation with adaptively chosen frequency samples is performed [17]. Since the device structure is a nonlinear frequency dependent BST varactor, the *frequency domain solver* was chosen for this type of simulation.

Before simulating the structure, the type of mesh must be considered due to its strong influence on the accuracy and speed of the simulation. The types of meshes which are typically selected are hexahedral mesh and tetrahedral mesh. In this case, tetrahedral mesh was implemented across the structure with local mesh refinements around the area of the electrodes as depicted in Figure 3. If hexahedral mesh is implemented, it may produce a large overhead in the number of elements for that part of the computational domain that does not require a fine mesh. For a small-scaled geometry such as the interdigital capacitor,

TABLE I. PARAMETER VALUES OF MODELLED BST IDC

Parameter	Value
Finger gap: f_G (μm)	1
Finger width: f_W (μm)	1
Finger length: f_L (μm)	110
Number of fingers: f_N	8
BST film thickness: h_{bst} (μm)	0.4
Sapphire thickness: h_{sub} (μm)	1.2
Electrode thickness: h_{elec} (μm)	2.0
Sapphire dielectric constant: ϵ_r	10.2

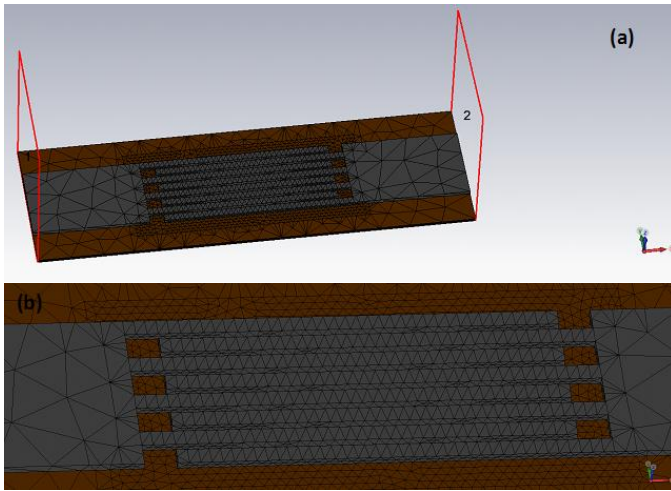


Fig. 3. Tetrahedral meshing with mesh refinements across the area of the modelled interdigital electrodes (a) Side view and (b) enlarge view of the tetrahedral meshing across the electrodes.

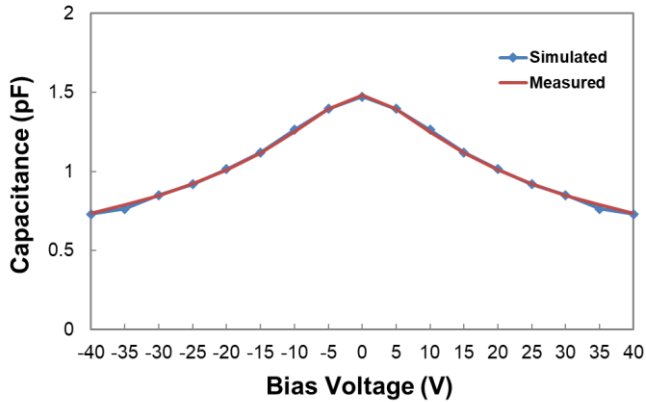


Fig. 4. Simulated and measured C-V curves of the BST varactor at 10 GHz.

tetrahedral mesh is more suitable as it does not include many mesh cells and can resolve the thin structure locally [17]. A total of ~27000 mesh elements were applied across the entire structure.

The simulation was subsequently performed by sweeping the dielectric constant of the defined BST thin film from 487 to 200 which corresponded to the bias voltage from 0 to 40 V of the measured BST varactor. The simulated and measured C-V curves at 10 GHz are shown in Figure 4 where excellent agreement is achieved.

III. PARAMETRIC ANALYSIS OF MODELLED BST STRUCTURE

In this section parametric analysis was performed by varying the IDC geometry and the changes in the shape of the nonlinear C-V curves were analysed. The aim of this analysis was to optimise the IDC parameter values for defining three distinct C-V curves: narrow, broad and intermediate curves.

In Figure 5, finger gap, f_G is varied from 1 to 10 μm while the other parameters such as finger width, f_W finger length, f_L and number of fingers, f_N are held constant at 1 μm , 110 μm

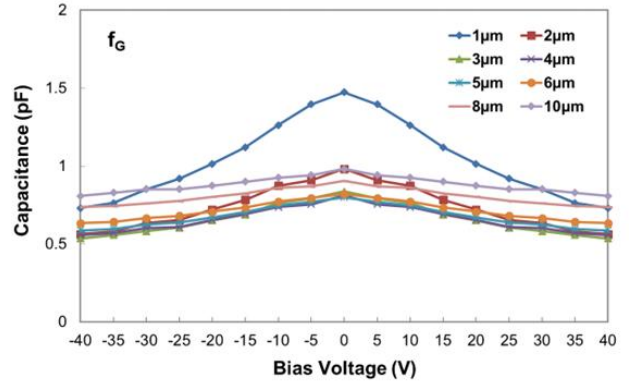


Fig. 5. The nonlinear C-V curves by varying the finger gap from 1 to 10 μm .

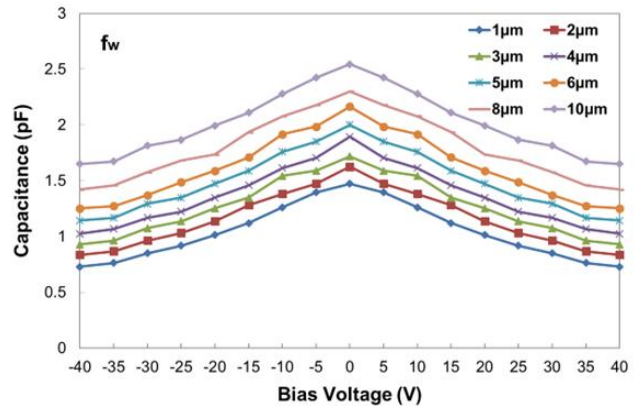


Fig. 6. The nonlinear C-V curves by varying the finger width from 1 to 10 μm .

and 8 respectively. As observed, the C-V curve becomes broader when f_G increases and the capacitance value drops over the entire tuning voltage range. This indicates a significant reduction in the tunability when f_G increases with the peak capacitance, C_{max} drops from 1.47 to 0.80 pF between 1 and 5 μm . Also, C_{max} drops significantly from 1 to 2 μm with a 0.49 pF difference. This notable difference can be attributed to the higher confinement of DC and microwave fields [5] in the BST film of the 1 μm finger gap, thus resulting in a higher tunability than the 2 μm finger gap. Notice that C_{max} escalates from 0.82 to 0.98 pF between 6 and 10 μm respectively. However, the reducing tunability trend occurs from 1 to 9 μm between 50.46 and 16.34 % but then a slight rise to 17.76 % at 10 μm .

Figure 6 shows the variation of finger width, f_W from 1 to 10 μm while the other parameters are fixed at $f_G = 1 \mu\text{m}$, $f_L = 110 \mu\text{m}$ and $f_N = 8$, resulting in an upward trend. As observed, the capacitance value increases uniformly over the entire tuning voltage range with C_{max} rises from 1.47 to 2.55 pF. However, the C-V curve becomes broader as f_W increases from 1 to 9 μm which reduces the tunability from 50.46 to 33.39 % but then slightly increases to 35.17 % at 10 μm .

In Figure 7, f_L is varied from 70 to 160 μm while $f_G = f_W = 1 \mu\text{m}$ and $f_N = 8$. An uptrend pattern is observed where the capacitance value increases uniformly over the entire tuning

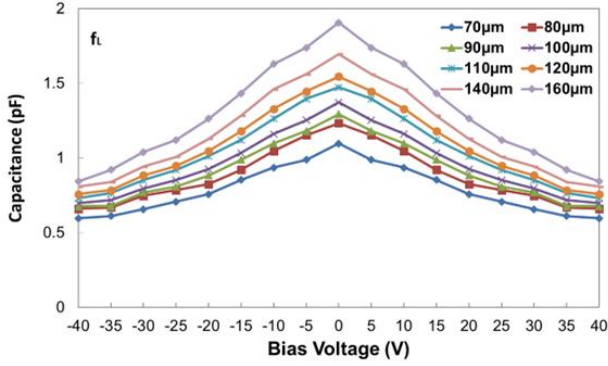


Fig. 7. The nonlinear C-V curves by varying the finger length from 90 to 150 μm .

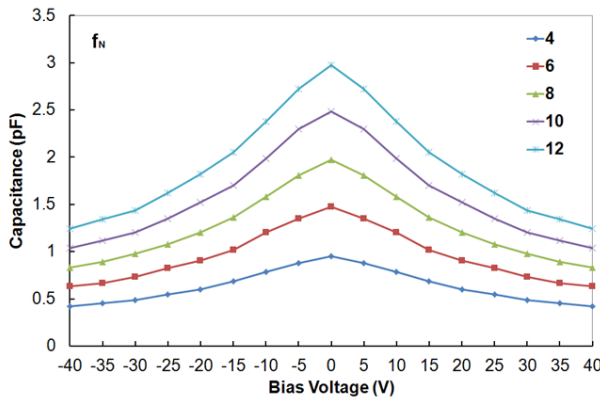


Fig. 8. The nonlinear C-V curves by varying the number of fingers from 4 to 12.

voltage range with C_{max} increases from 1.10 to 1.91 pF. However, in contrast to Figure 6, the C-V curve becomes narrower which increases the tunability from 45.70 to 55.71 %.

Figure 8 also indicates that by varying f_N from 4 to 12 with constant parameters at $f_G = f_W = 1 \mu\text{m}$ and $f_L = 110 \mu\text{m}$, C_{max} increases from 0.95 to 2.97 pF and the C-V curve becomes narrower. However, this trend has a slight impact on the tunability, which is about 2% rise from 4 to 12.

IV. 1 DB COMPRESSION POINT OF BST VARACTOR

From the parametric analysis shown in the previous section, the narrow, broad and intermediate C-V curves were extracted and 1 dB compression points for all cases were determined. The IDC geometry for each case was optimised with C_{max} value preserved at ~ 1.47 pF as depicted in Figure 4.

Table II shows the optimised parameter values for each case. For the narrow curve, the IDC geometry was chosen to achieve the highest tunability of 50.5 %. This was well in agreement with [5] where the highest degree of confinement of DC and microwave fields in the BST film can be realised due to $f_g \approx f_w$ with the smallest values. The IDC geometry for the broad curve was chosen to achieve the lowest tunability at 13.6 %. In this case, the lowest confinement of DC and microwave fields in the BST film was realised due to the largest values of f_g and f_w .

Figure 9 shows the electric field distributions between the

TABLE II. PARAMETER VALUES OF NARROW, BROAD AND INTERMEDIATE C-V CURVES

Parameter	Narrow	Broad	Intermediate
Finger gap: f_G (μm)	1	10	7
Finger width: f_W (μm)	1	10	7
Finger length: f_L (μm)	110	155	160
Number of fingers: f_N	8	8	8
Simulated capacitance (pF)	0 V	1.47	1.47
	40 V	0.73	1.27
Simulated tunability (%)	50.5	13.6	26.2

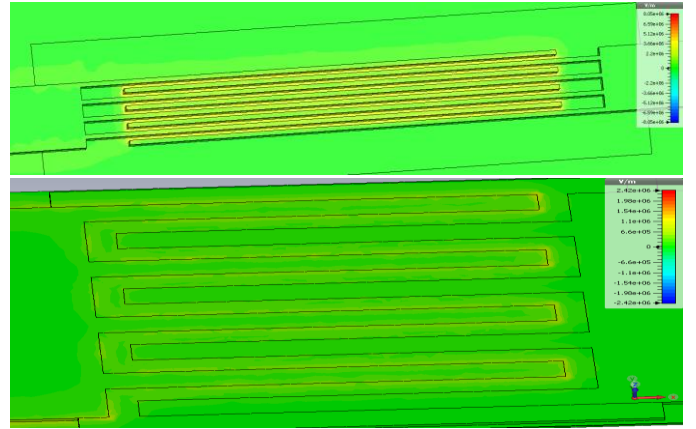


Fig. 9. Electric field distributions between the 1 μm and 10 μm gap varactors.

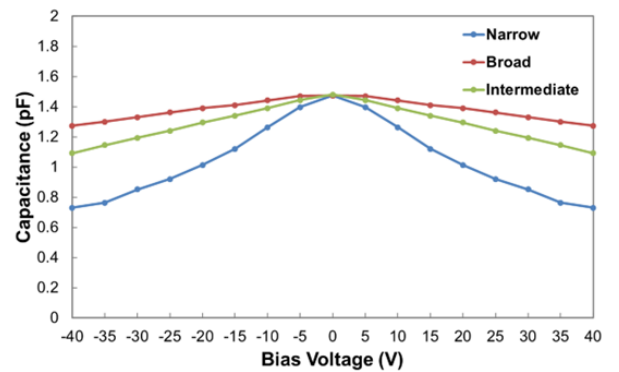


Fig. 10. Simulated narrow, broad and intermediate nonlinear C-V curves.

gaps of the electrodes for the narrow and broad varactors. As observed, high intensity of E-fields (indicated with dark orange colour) occurs between the 1 μm gaps while considerably less E-fields intensity is expected between the 10 μm gaps. The IDC geometry for the intermediate curve achieved a tunability of 26.2 %. All the curves are depicted in Figure 10.

The data in Figure 10 was subsequently compared to the established nonlinear C-V BST varactor model [18] via a curve-fitting function in MATLAB. A very good fit was achieved and

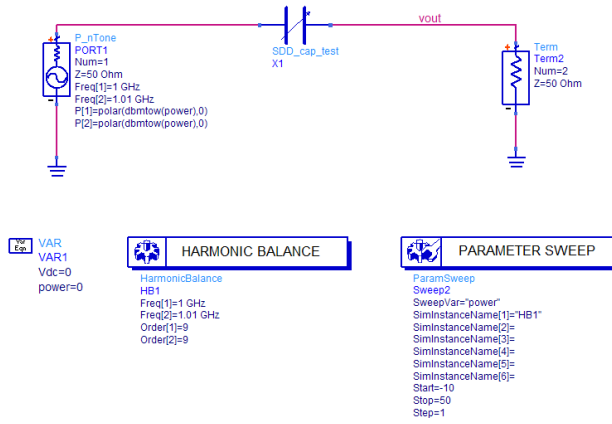


Fig. 11. The nonlinear equation-based capacitor in a two-port series network for determining the 1 dB compression point.

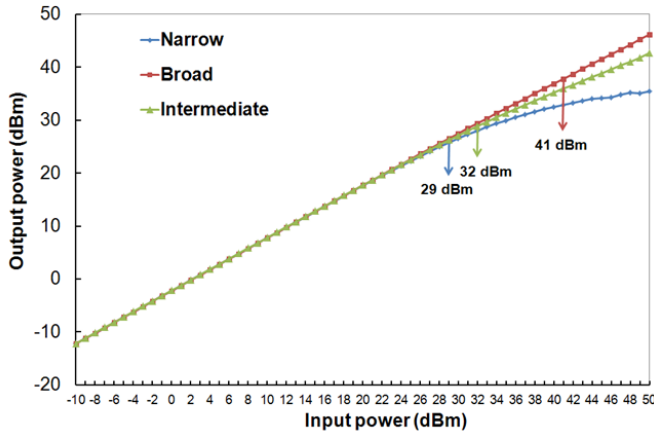


Fig. 12. The 1 dB compression point of the simulated narrow, broad and intermediate C-V curves.

important parameter values of the fringing capacitance (C_f) and the “2:1” voltage (V_2) were extracted. Using Agilent Advanced Design System (ADS) software, this nonlinear model along with the extracted parameter values were substituted into a nonlinear equation-based capacitor of a simple two-port series network as designed in Figure 11. The simulation was then performed by varying the input power from -10 to 50 dBm and the 1 dB compression point for each C-V curve was determined.

Figure 12 shows the 1 dB compression points for the narrow, broad and intermediate C-V curves. As observed, the broad curve achieves the highest 1 dB compression point at 41 dBm compared to the narrow and intermediate curves at 29 and 32 dBm respectively. Even though the broad curve could withstand higher input power levels, it is compensated by having the lowest tunability. In contrast, the narrow curve compresses at lower input power levels but achieves the highest tunability. However, a BST varactor with reasonably high tunability and 1 dB compression point could be realised with the intermediate curve.

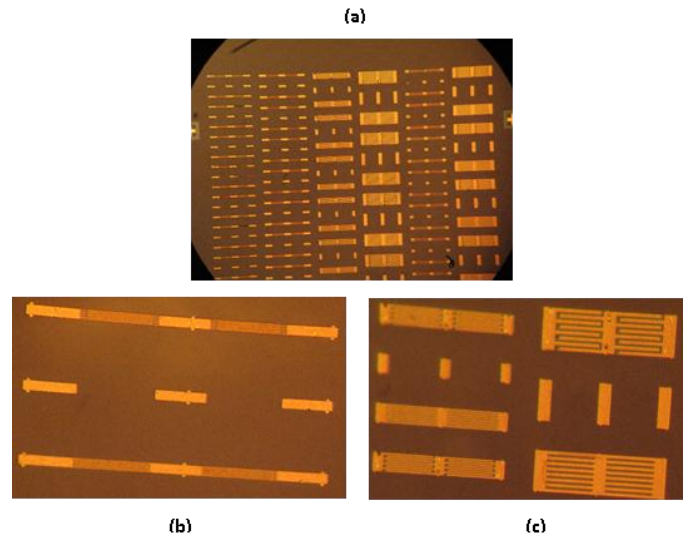


Fig. 13. (a) The whole fabricated BST thin film varactors with different geometries on c-plane substrate, (b) the narrow varactor and (c) the intermediate and broad varactors on the left and right sides respectively.

TABLE III. PERFORMANCE OF MEASURED NARROW, BROAD AND INTERMEDIATE VARACTORS AT 10 GHz

Type of varactor	Narrow		Broad		Intermediate	
Bias voltage (V)	0	40	0	40	0	40
Capacitance (pF)	1.4805	0.7365	0.4927	0.463	1.0876	0.8219
Q-factor	8.74	20.76	16.3	24.6	12.6	22.23
Tunability (%)	50.25		6.04		24.4	

V. MICROWAVE MEASUREMENTS OF BST VARACTOR

All the optimised C-V curves were realised in the physical form of varactors. The narrow, broad and intermediate varactors were fabricated on the deposited 400 nm BST layer grown on c-plane sapphire substrate. The details of the material deposition and fabrication process were comprehensively discussed in [19]. Figure 13 shows the fabricated BST thin film varactors. Microwave measurements were performed and the results for all three varactors are tabulated in Table III.

Figure 14 shows the measured C-V curves for all three varactors. As observed, the measured C_{max} (0 V) for the broad and intermediate varactors were lower than ~ 1.47 pF of the equivalent simulated results and the tunabilities were also degraded due to the broader shape of the curves. The major constraint identified was strain-induced film due to the existence of oxygen vacancies which contributed to the lower tunability of the varactors. In this case, thinner film usually has a higher tensile strain and reduced grain size, which contributes to the lower dielectric constant. However, it was reported that the BST thickness could be optimised to achieve strain-relieved film with the highest tunability [20]. Post-annealing the film in air assisted in improving the quality of the film, making it more crystalline and significantly reducing strain in the film.

The measured data for all varactors from Figure 14 were compared to the established nonlinear BST model and substituted in the network similar to Figure 11. Simulation was

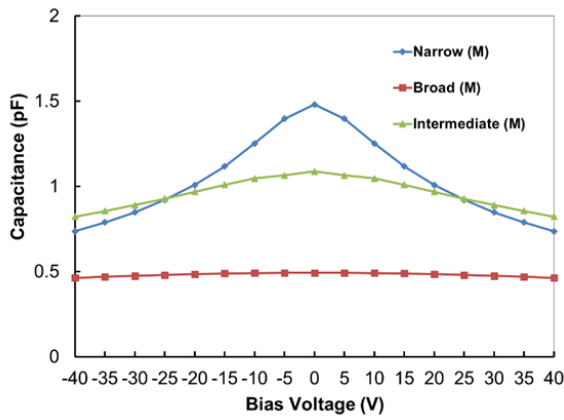


Fig. 14. The nonlinear C-V curves of the measured (M) narrow, broad and intermediate varactors.

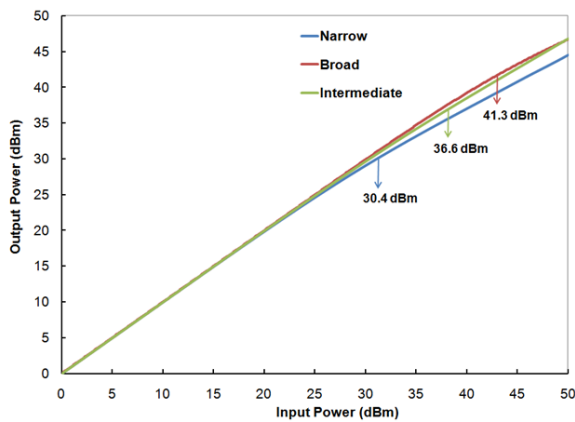


Fig. 15. The 1 dB compression point of the measured narrow, broad and intermediate varactors.

TABLE IV. RELATIONSHIP BETWEEN TUNABILITIES AND 1 dB COMPRESSION POINTS OF THE VARACTORS

Type of varactor	Narrow		Broad		Intermediate	
	S	M	S	M	S	M
Tunability (%)	50.46	50.25	13.6	6.04	26.21	24.4
1 dB compression point (dBm)	29	30.4	41	41.3	32	36.6

S = Simulated, M = measured

performed and the 1 dB compression point for each varactor was extracted as depicted in Figure 15.

Table IV shows the relationships between tunabilities and 1 dB compression points for all measured and simulated varactors. As observed, the tunabilities of the measured varactors had dropped compared to their respective simulated varactors mainly in the broad varactor. It is evident that C_{max} along with the tunability for each varactor had changed. However, the extracted 1 dB compression points for the measured varactor results were comparable to the simulated results. Although the intermediate varactors had a 4.6 dB difference between them, this could be attributed to the much broader curve of the measured intermediate varactor and a slight fabrication issue. The relationship between the tunability

and the 1 dB compression point is still valid; the varactor with the highest tunability produces the lowest 1 dB compression point while varactor with the lowest tunability produces the highest 1 dB compression point.

VI. CONCLUSION

This paper has presented the relationship between the tunability and the 1 dB compression point of a BST varactor. The interdigital capacitor was modelled using CST software and a parametric analysis was made of its geometry by varying the finger gap, finger width, finger length and number of fingers in the specified design range. The effects on the shape of the nonlinear C-V curves were analysed for each parameter variation and three distinct C-V curves of narrow, broad and intermediate curves were subsequently produced. The 1 dB compression points for the optimised C-V curves were finally extracted from simulation.

For the equivalent fabricated varactors, the measured tunability for each varactor was lower than the simulated results especially in the broad varactor due to strain-induced film. However, the 1 dB compression points extracted for all three measured varactors were still comparable with the simulated results. These BST varactors have the potential to be implemented in high power microwave systems, possibly by integrating them with standard semiconductor chips and form hybrid modules such as system-on-chip (SoC).

ACKNOWLEDGMENT

The authors would like to thank the RMIT University for providing the lab facilities.

REFERENCES

- [1] S. K. Nath et. al., "A Highly Tunable Barium Strontium Titanate Thin Film MIM Varactor With Floating Metal," *IEEE Microw. Wireless Comp. Lett.*, vol. 31, no. 12, pp. 1283-1286, Dec. 2021.
- [2] S. Abdulazhanov et. al., "Permittivity Characterization of Ferroelectric Thin-Film Hafnium Zirconium Oxide Varactors up to 170 GHz," 2023 Device Research Conference (DRC), Santa Barbara, CA, USA, 2023, pp. 1-2.
- [3] V. Muzzupapa et al., "Frequency Reconfigurable Millimeter Wave Antenna Integrating Ferroelectric Interdigitated Capacitors," 2023 17th European Conference on Antennas and Propagation (EuCAP), Florence, Italy, 2023, pp. 1-4.
- [4] W. Xian-Kui et. al., "Progress on Emerging Ferroelectric Materials for Energy Harvesting, Storage and Conversion," *Advanced Energy Materials*, vol. 12, no. 2201199, pp. 1-22, June 2022.
- [5] S. Gevorgian, *Ferroelectrics in Microwave Devices, Circuits and Systems: Physics, Modelling, Fabrication and Measurements*, 1st ed. London: Springer, 2009.
- [6] P. Jeevankumar et. al., "Fabrication of Ba_{0.5}Sr_{0.5}TiO₃ components combining rapid prototyping with gelcasting using different gelling systems," *Open Ceramics*, vol. 17, no. 100152, pp. 1-9, Nov. 2023.
- [7] P. Bouca et. al., "Reconfigurable Three Dimension Single and Dual-Band SDR Front-Ends Using Thin Film BST-Based Varactors," *IEEE Access*, vol. 10, pp. 4125-4136, 2022.
- [8] P. Bouca et. al., "Design and Characterization of Novel Barium Strontium Titanate Thick Films for Sub-6 GHz RF Applications," *IEEE Trans. Microw. Theory Techn.*, vol. 70, no. 1, pp. 611-621, Jan. 2022.
- [9] S. Nam et. al., "A Switchless Quad Band Filter Bank Based on Ferroelectric BST FBARs," *IEEE Microw. Wireless Comp. Lett.*, vol. 31, no. 6, pp. 662-665, June 2021.

- [10] C. Tong et. al., "Compact Wideband Circularly Polarized Dielectric Resonator Antenna With Dielectric Vias," *IEEE Antennas Wireless Propag. Lett.*, vol. 21, no. 6, June 2022.
- [11] M. Z. Koochi and A. Mortazawi, "Reconfigurable Radios Employing Ferroelectrics: Recent Progress on Reconfigurable RF Acoustic Devices Based on Thin-Film Ferroelectric Barium Strontium Titanate," in *IEEE Microwave Magazine*, vol. 21, no. 5, pp. 120-135, May 2020.
- [12] C. Schuster et al., "Concept for Continuously Tunable Output Filters for Digital Transmitter Architectures," *IEEE Access*, vol. 7, pp. 123490-123504, 2019.
- [13] D. Kienemund et. al., "Suppression of Acoustic Resonances in Fully-Printed, BST Thick Film Varactors Utilizing Double MIM Structures," 2018 48th European Microwave Conference (EuMC), Madrid, Spain, 2018, pp. 567-570.
- [14] D. Kienemund et al., "Acoustical Behavior of Fully-Printed, BST MIM Varactor Modules in High Power Matching Circuits," 2018 IEEE/MTT-S International Microwave Symposium - IMS, Philadelphia, PA, USA, 2018, pp. 1393-1396.
- [15] S. Preis et al., "A High-Efficiency GaN Transistor Module with Thick-Film BST-Based Tunable Matching Network," 2018 48th European Microwave Conference (EuMC), Madrid, Spain, 2018, pp. 1-4.
- [16] M. F. Abdul Khalid, A. S. Holland and K. Ghorbani, "Influence of post-annealing on the performance of BST thin film varactors," 2014 Asia-Pacific Microwave Conference, Sendai, Japan, 2014, pp. 309-311.
- [17] CST, "Waveguide Port Overview Documentation," ed, 2012.
- [18] D. R. Chase, Lee-Yin Chen and R. A. York, "Modeling the capacitive nonlinearity in thin-film BST varactors," in *IEEE Trans. Microw. Theory Techn.*, vol. 53, no. 10, pp. 3215-3220, Oct. 2005.
- [19] M. F. Abdul Khalid., "Investigation of large-signal performance on BST varactors for microwave device applications", Ph.D. dissertation, School of Electrical and Computer Engineering, College of Science, Engineering and Health, RMIT University, Melbourne, 2014.
- [20] E. A. Fardin., A.S. Holland and K. Ghorbani, "Polycrystalline Ba_{0.6}Sr_{0.4}TiO₃ thin films on r-plane sapphire: Effect of film thickness on strain and dielectric properties," *Applied Physics Letters*, vol. 89, Oct. 2006.